Supporting Information

Edwards et al. 10.1073/pnas.1219701110

SI Methods

Expression and Purification of the Nicking Enzyme in *Staphylococcus aureus* Relaxase Domain. Cloned constructs were transformed into chemically competent *Escherichia coli* BL21 (DE3) AI cells. Transformed cells were grown in 1.5 L of lysogeny broth (LB), in the presence of ampicillin, at 37 °C, with shaking, to an optical density of 0.6–0.8. An L-Arabinose solution was added to the growth at a final concentration of 0.2% (vol/vol), and the temperature was reduced to 18 °C for 30 min. Protein expression was induced with 100 μM isopropyl-β-D-thiogalactopyranoside (IPTG) and cells were allowed to grow for 16 h. The resulting growths were spun at 4,500 × *g* for 30 min at 4 °C and split into six pellets that were stored at −80 °C. Individual pellets were resuspended in nickel A buffer [500 mM NaCl, 25 mM imidazole, 20 mM potassium phosphate buffer, pH 7.4, and 0.02% (vol/vol) sodium azide] along with protease inhibitor tablets (Roche), DNase, and lysozyme. The slurry was lysed using a Fisher Scientific Sonic Dismembrator at 50% power for three cycles of 1 min with 1-s intervals at 4 °C. The lysed cells were then spun at 18,500 × *g* for 1 h. The supernatant was filtered and purified over a HisTrap column (GE Healthcare). None of the N-terminal His_6 or His_6 MBP constructs expressed solubly after the removal of the tag by tobacco etch virus (TEV) protease. The CPD constructs were allowed to bind to the HisTrap column and incubated with $InsP_6$ for 3 h at 4 °C. The resulting protein was then further purified over a Superdex 200 column (GE Healthcare) preequilibrated in sizing buffer [300 mM NaCl, 50 mM Tris buffer, pH 7.4, and 0.02% (vol/vol) sodium azide]. Fractions containing nicking enzyme in *Staphylococcus aureus* (NES) 1–220, which was found to contain the functional and soluble relaxase domain of NES, were combined and used for site-directed mutagenesis as well as for the following experiments.

To obtain protein in complex with DNA an active site mutant Y25F was used. A piece of DNA with the sequence 5′-ACGCGAACGGAACGTTCGCATAAGTGCGCC-3′ was synthesized (IDT) and used as the substrate. After nickel purification the DNA was added in a 2.25-M excess to the enzyme and size exclusion chromatography was performed for final purification. The presence of DNA was confirmed by measuring the absorbance of $A_{260/280}$ on a nanodrop (Thermo Scientific).

Relaxase–DNA Complex Structure Determination. Selenomethionine-substituted protein was used in crystal trials to obtain phase information upon data collection. NES 1–220 + DNA (10 mg/mL) was crystallized in a solution containing 16% (vol/vol) PEG-8000, 120 mM calcium acetate, 80 mM sodium cacolydate (pH 6.5), and 20% glycerol (vol/vol). The trays were set with drop ratios of 1:1, 1:2, and 2:1 of protein to mother liquor, respectively. Vapor diffusion hanging-drop trays were set at 20 °C to obtain well-formed crystals. The crystallization solution was found to be an adequate cryoprotectant in subsequent diffraction experiments performed at the University of North Carolina (UNC) Biomolecular X-ray Crystallography Facility. The crystals were flash frozen in liquid nitrogen for data collection at 100 K.

Datasets were obtained on the 23_ID_B beamline maintained by the National Institute of General Medical Sciences and the National Cancer Institute Collaborative Access Team (GM/CA-CAT) at the Advanced Photon Source (APS) part of the Biosciences Division (BIO) at Argonne National Laboratory (ANL). A fluorescence scan was performed at the selenium absorption edge to confirm that the selenomethionine substitution was successful. The collection strategy used included 1-s exposures with a 1° rotation between frames and an inverse beam every 10° to collect 100° of data. The datasets were indexed and scaled using HKL-2000 processing software (1). Indexing resulted in a space group of $P6_422$ with one NES relaxase–DNA complex per asymmetric unit. The best data were obtained when the resolution was cut to 2.9 Å. Initial phases were determined using the Phenix software suite with the AutoSol function (2). Two of the three heavy atom sites were successfully located. This was a result of the first amino acid, methionine, not being observable in the final structure, most likely as a result of it being processed away during expression as was seen in the MobA structure (3). The model was built using Coot (4) by placing the selenomethionines and iteratively building the protein from these starting points. Refinements were performed using the Phenix refine application (2).

Expression and Purification of the NES C-terminal Domain. The NES C-terminal domain was predicated to be helical but did not have a large region of homology to any protein of known structure. Therefore, a number of constructs encoding all or some of the C-terminal domain of NES were tested for expression, solubility, and ability to crystallize. The best was NES 243–594, but original crystals of this construct were mosaic and poorly diffracting (>4 Å). One patch of surface entropy reduction mutants was created: EKE 178–180 to AAA 178–180. This protein was cloned and expressed as a C-terminal CPD fusion with a 6-His tag at the C terminus of CPD in *E. coli* BL21 (DE3) AI cells. Fresh transformants were cultured in "Terrific Broth," in the presence of ampicillin, to an optical density of 0.6–0.8, at 37 °C. The temperature was then reduced to 18 °C and arabinose added, followed by 0.1–2 mM IPTG. Cells were harvested by centrifugation, lysed by sonication in Nickel column buffer "A", 50 mM potassium phosphate (pH 7.4), 500 mM NaCl, and 25 mM imidazole, and the soluble fraction was collected by a high-speed centrifugation and filtered through a 0.22-μm membrane. This was bound via the C-terminal His-tag on CPD to a 5.0-mL GE Healthcare His-Trap column. After the unbound cellular proteins were washed out of the column with buffer A, 2 mM $InsP_6$ was injected onto the column and allowed to incubate for 2–3 h. The cleaved NES 243–594 was eluted in Nickel buffer A; this usually included a small amount of uncleaved fusion protein as well as some CPD. Fractions containing this mixture were then passed over a Superdex 200 size exclusion column in 50 mM Tris (pH 7.4), 300 mM NaCl. Peak fractions contain the cleaved NES 243–594. For preparing selenomethionine-substituted protein, protein was expressed in the *E. coli* methionine auxotroph B834 in SelenoMet Medium Base (Athena Enzyme Systems) supplemented with selenomethionine (Anatrace) according to the manufacturer's instructions.

The C-terminal domain protein was screened for crystallization at the UNC Macromolecular X-ray Crystallography Core Facility, using a PHOENIX 96-well crystallization robot. Rod-shaped crystals grew in numerous conditions containing PEG-4000 or PEG-6000. These were optimized and cryoprotectants were added into the growth conditions, such that the final crystallization mixture contained 12–16% (wt/vol) PEG-6000, 0.1 M Tris·HCl (pH 8.0), 0.5 M LiCl, 12.5% (vol/vol) glycerol, and 5% (vol/vol) PEG-400. Crystals were grown in hanging-drop trays at 22 °C.

C-Terminal Domain Structure Determination. Selenomethionyl NES 243–594 crystals were flash-frozen in liquid nitrogen and shipped to the Advanced Photon Source for remote data collection at GM/CAT Beamline 23 ID-B. Fluorescence scans revealed strong signal at the selenium absorption edge; therefore, SAD and MAD datasets were collected. Data were integrated and scaled with the software XDS (5). The structure was solved using a MAD dataset collected using a single crystal with three identical 120° scans at the peak (12.661 kEV), inflection (12.658 kEV), and remote (13.061 kEV) X-ray wavelengths. The crystals were large (200 μm thick and up to 1 mm length) but mosaic; therefore, the minibeam at 23 ID-B was set to 20 μm and was used to collect less mosaic datasets, and the beam was moved to a new region of the crystal at each new wavelength. This reduced the mosaicity from well above 1° to 0.5–0.6°. Selenium atom sites were found and density modification was carried out using "SOLVE/RESOLVE" under PHENIX; only five of seven Se sites per monomer were reproducibly located. Initial experimentally phased maps indicated strong helical density. A model was partially built using PHENIX, and, using the selenium sites as reference, much of the amino acid chain was traced manually. The N-terminal 10 aa are not visible in the maps and are therefore disordered. Two of the seven Se-Met residues are in that sequence. Once most of the model was built, refinement was initiated in PHENIX, using the remote wavelength dataset for refinement. Therefore, the methionine residues are built as selenomethionine. Experimental phase restraints were used initially, as well as translation, libation, screw (TLS) restraints in the latter stages of refinement. Three groups of residues were chosen as separate TLS groups on the basis of the following: (*i*) Two of these are structural repeats 254–366 and 367–514, and (*ii*) the third is a small domain (residues 515–594) at the end of the structure. We included hydrogen atoms built by PHENIX "ready-set" in the refinement so that proper packing constraints could be maintained throughout. Even so, certain regions of the electron density are weak, with high B-factors (the mean isotropic B-factor is 70.5) and some side chains not visible. Such residues are built as Alanine "stubs" in the final model but labeled as their proper name in the coordinate file.

DNA-Binding Studies: Direct Binding. To determine whether the relaxase bound DNA in a specific, high-affinity fashion we used fluorescence anisotropy to measure the interaction. NES relaxase and the NES relaxase Y25F mutant were used to determine the dissociation constant, K_D, for the initial probe used. The annealed DNA oligonucleotide selected for the initial experiments had the sequence 5′ 6-FAM-ACGCGAACGGAACGTTCGCATAAGTGCGCC 3′ that incorporated the full inverted repeat and the 5′ side of the hypothesized *nic* site (terminal C base). For each assay, purified protein was diluted to 2× maximal assay concentration into a buffer of 150 mM NaCl, 0.1 mg/mL BSA, 5 mM Mg^{2+} Acetate, 25 mM Tris Acetate, pH 7.5. The protein stock was then serial diluted into 40 μL of the final reaction buffer (100 mM NaCl, 0.1 mg/mL BSA, 5 mM Mg^{2+} Acetate, 25 mM Tris Acetate, pH 7.5). This was done in a 384-well black assay plate (Costar) to generate 16 concentrations of protein, 8 dilutions from 500 nM protein and 8 from 400 nM protein. The DNA probe was diluted to 5× final assay concentration into the reaction buffer. Ten microliters of the DNA stock solution was added to the 40 μL, resulting in a final concentration of DNA probe at 50 nM, 1× protein, and a total volume of 50 μL in each well. The no-protein control well was generated by adding 10 μL DNA to 40 μL reaction buffer.

Fluorescence anisotropy (FA) was used to measure the dissociation constant for the DNA oligo. The FA of the fluorescently labeled substrate at 520 nm was measured following excitation at 485 nm, using a PHERAstar plate reader (BMG Labtech) in a T format. Measurements were made in triplicate and the normalized data were plotted as average FA vs. protein concentration. Eq. **S1** was used to fit the data, using Graphpad PRISM v5.03 (Graphpad, 2010), and to calculate the K_D for the substrate,

$$f = min + (max - min)\frac{\left\{(T + x + K) - \left[(-T - x - K)^2 - 4Tx\right]^{\frac{1}{2}}\right\}}{2T}, \qquad \textbf{[S1]}$$

where f is average FA signal detected; T, total DNA concentration (set to 50 nM); x, total protein concentration; K, K_D; *min*, average FA signal of no protein control; and *max*, average FA signal of sample at saturating concentration of protein. A single binding site was assumed and all experiments were run in triplicate with SE reported for each measurement.

DNA-Binding Studies: Competition Binding. To determine the effect of altering the DNA substrate sequence, DNA competition assays were used. Again, fluorescence anisotropy was measured, this time to determine the effect of unlabeled competitor oligonucleotides on the dissociation constant of the substrate used in the direct-binding studies. The assay was setup in a similar fashion to that in the direct-binding studies except the protein and labeled DNA oligonucleotides were held constant and the unlabeled competitive oligonucleotide was titrated. The same 384-well assay plate was used in the experiment. The final reaction buffer was the same (100 mM NaCl, 0.1 mg/mL BSA, 5 mM Mg^{2+} Acetate, 25 mM Tris Acetate, pH 7.5) with the addition of the labeled DNA oligonucleotide at 62.5 nM. The labeled DNA oligonucleotide was also added to the unlabeled stock of competitor oligonucleotide at 125 nM so that the concentrations were not affected during titration. The maximal 2× concentration for the competitor oligonucleotide was 20 μM. As in the direct-binding experiments, 40 μL of the final reaction buffer was placed in each of the 16 wells. For the competition experiments, 40 μL of the competitor oligonucleotide was sequentially titrated down to the final concentration. The final well contained the no-protein control that contained only reaction buffer and labeled and unlabeled competitor oligonucleotide. Finally, 10 μL of protein at 5× reaction concentration was added to the wells. This resulted in an assay with 100 nM protein, 50 nM labeled DNA oligonucleotide, and a titration of competitor oligonucleotide concentrations from 10 μM to 0 μM. Reductions in anisotropy were measured using the PHERAstar plate reader (BMG Labtech) in a T format. Measurements were made in triplicate and the normalized data were plotted as average FA vs. log protein concentration. Eq. **S2** was used to fit the data, using Graphpad PRISM v5.03 (Graphpad, 2010), and to calculate the IC_{50} for the competitor,

$$f = min + (max - min) \Big/ \left[1 + 10^{(x - LogIC_{50})}\right], \qquad \textbf{[S2]}$$

where f is the average FA signal detected; x, the competitive oligo concentration; $LogIC_{50}$, the concentration at which the maximal signal has decreased by half; *min*, average FA signal of no-protein control; and *max*, average FA signal of the sample at the saturating concentration of protein. Once the IC_{50} has been determined, it can be used in the following equation to determine the dissociation constant for the inhibitor (K_i), using Eq. **S3**,

$$K_i = [I]_{50} \Big/ \left(\frac{[L]_{50}}{K_d} + \frac{[P]_0}{(K_d + 1)} \right), \quad \text{[S3]}$$

where K_i is the dissociation constant for the inhibitor; $[I]_{50}$, the concentration of free inhibitor at 50% inhibition; $[L]_{50}$, the concentration of free labeled ligand at 50% inhibition; $[P]_0$, the concentration of free protein at 0% inhibition; and K_d, the dissociation constant of the protein–ligand complex (6, 7). All experiments were run in triplicate with SE reported.

NES Equilibrium DNA Cleavage-Religation Assays. Commercially synthesized *oriT* DNA substrates (IDT) were ordered with 5′ 6-FAM fluorescein molecules attached. Each 10-μL reaction contained 5.37 μM NES protein, 1 μL of 10 μM 5′ 6-FAM–labeled DNA substrate, and EMSA buffer [50 mM NaCl, 20 mM Tris, pH 7.4, 0.02% (vol/vol) sodium azide]. The reaction was incubated at 37 °C for 1 h and quenched with the addition of 10 μL 2× quenching solution (0.01% xylene cyanol, 85% formamide, 20 mM EDTA, 2× TAE, 0.2% SDS). The 20 μL were run through a denaturing 16% polyacrylamide gel [40 mL 16% acrylamide gel stock (8 M urea, 16% polyacrylamide/bisacrylamide, 1× TBE), 400 μL 10% ammonium persulfate (APS), 40 μL tetramethylethylenediamine (TEMED)] in 1× TBE running buffer to separate the substrate and products. The fluorescent oligos were visualized using a VersaDoc Imaging System, 4400 MP (BioRad), and the accompanying Quantity One software (BioRad). Band intensities were quantified using ImageJ 1.42 software. Before quantification, standard background subtraction was performed on all gels. The protein was determined to be active if the smaller product band was present in the gel. Activity was reported as a percentage of the product band intensity divided by the product plus substrate intensities.

For the metal studies it was necessary to remove the natively bound metal through incubation of NES relaxase in 500 μM EDTA overnight at 4 °C. The metals of interest were then added in 10-, 100-, and 1,000-μM excess and activity was measured. The reaction conditions for the metal studies contained 7 μL of EMSA buffer (50 mM NaCl, 20 mM Tris, pH 7.4, 0.02% vol/vol sodium azide), 1 μL of 50 μM NES relaxase in sizing buffer incubated in 500 μM EDTA, 1 μL of 10 μM 5′ 6-FAM–labeled DNA substrate, and 1 μL of the metal in EMSA buffer at 10× the desired fold excess. The reaction was incubated at 37 °C for 1 h and quenched with the addition of 10 μL 2× quenching solution (0.01% xylene cyanol, 85% formamide, 20 mM EDTA, 2× TAE, 0.2% SDS). Gels were run in the same fashion as for the *nic* site studies.

Inductively Coupled Plasma Mass Spectrometry. NES relaxase and NES relaxase H131A mutant were analyzed by inductively coupled plasma mass spectrometry (ICP-MS) to determine the identity and concentration of metals present in the samples. Data were collected by the UNC-Chapel Hill Chemistry Department Mass Spectrometry Core Facility on a Varian 820-MS. Protein was first digested for 4 h in 70% nitric acid (HNO_3). Each sample was then diluted in 5.5 mL of 1.4% HNO_3. Data were collected as parts per billion (ppb) and converted to μM. The original concentration of each metal in each sample was then determined in Excel 2007 (Microsoft, 2011). Data were then presented as percentage bound of the total concentration of protein.

Small-Angle X-Ray Scattering. Purified full-length Y25F NES protein was combined with the 32-bp sequence including the oriT hairpin and passed over a Superdex 200 gel filtration column in 50 mM Tris·HCl (pH 7.4), 300 mM NaCl. Fractions containing NES+DNA complex were pooled, concentrated to greater than 10 mg/mL, and flash-frozen in liquid nitrogen. Gel filtration flow-through was collected for small-angle X-ray scattering (SAXS) buffer subtraction. Samples and buffer were shipped overnight on dry ice to RigakuUSA and stored at −80 °C until data collection. Samples were thawed at 4 °C and centrifuged at 10,000 × *g* for 10 min. Twenty-three–microliter samples of buffer and protein were placed into a quartz capillary sample holder for SAXS data collection at ambient temperature. The Rigaku Bio-SAXS 1000 instrument (including FR-E+ generator, Kratky camera, and Pilatus 100K hybrid pixel array detector) was used to collect 60-min scans at three protein concentrations (10.6, 5.3, and 2.65 mg/mL). Each scan was the sum of six 10-min contiguous exposures to monitor for radiation-induced changes in scattering; for these samples, no detectable changes in R_g occurred between the first and last 5-min exposures at all concentrations. Sample and buffer images were converted from pixel space to *q*-space and averaged to produce 1D plots of "I vs. q," using SAXSLab calibrated with an AgBeh standard. Buffer plots were subtracted from sample plots in the SAXSLab software.

Radius of gyration values were calculated using both PRIMUS and GNOM from the ATSAS software, using the Guinier plots ($0.68 < \sigma R_g < 1.3$) and real space pairwise distance distribution function (PDDF) plots. The Guinier R_g value was consistently between 36.5 and 37.8 Å for all three protein concentrations and the PDDF R_g was 37.9–38.7 Å. Fig. S4*A* shows the pairwise-distribution function plot for the highest concentration. The fact that these values did not change with concentration and that the calculated intensity at 0 s (I_0) is completely linear with concentration show that the samples did not aggregate within this concentration range. Kratky plots of the data showed typical folded protein character. The SAXS curves and Guinier analysis of NES 228–665 (the C-terminal domain) and the NES 1–220 + DNA complex had concentration-dependent R_g values and displayed some aggregation effects; these data were not used further. The SAXS-derived molecular mass of the complex was calculated using both datPOROD and SAXSMoW; the values obtained were between 76 kDa and 92 kDa. A monomer of full-length NES+DNA has a calculated MW of 89 kDa, well within the range determined from the SAXS data. This also confirms that the protein–DNA complex is a monomer in solution, a result suggested previously by gel filtration.

The MONSA algorithm (8) was used to calculate dummy atom models from which we created the two-phase molecular envelope shown in Fig. 3*D* in which the Chimera (9) molecular surfaces generated from the averaged protein (light pink) and DNA (light yellow) phases were calculated from 10 runs of MONSA. These MONSA calculations used two curves: a calculated SAXS curve for the DNA from our crystal structure of the NES relaxase–DNA complex and the experimental curve containing the full-length protein bound to DNA. The 10 MONSA dummy atom models had a mean normalized spatial discrepancy of 0.921 ± 0.058; 1 of 10 was discarded. The calculated vs. experimental SAXS curve for the dummy atom model most similar to all of the rest ($\chi = 1.16$) is shown in Fig. S4*B* (red curve). We carried out rigid-body modeling of NES 1–195 + DNA crystal structure and NES 253–593 crystal structure, using SASREF (10) to find configurations that match the SAXS data (Fig. S4*B*, blue curve). Using 30–40 Å as a distance constraint between the last visible amino acid residue in the N-terminal domain (195) and the first visible amino acid in the C-terminal domain structure (253), a top docked model is shown in the SAXS envelope in Fig. 3*D*.

Conjugation Assays in *S. aureus*.
Bacterial strains, plasmids, and growth conditions

	Description	Source
RN4220	Restriction-deficient derivative of NCTC 8325	(11)
SK5428	SK982 harboring pSK41	(12)
SK8046	Tc^R; RN4220, pYLΔ112 with *rep* integrated in *geh*	(13)
SK6872	RN4220 harboring pSK41::nes2	This study
pNL9164	*Staphylococcus aureus* Targetron vector	(14)
pSK41	46-kb conjugative multiresistance plasmid	(15)
pSK5632	Cm^R; pSK1 shuttle vector	(16)
pSK6873	pSK5632 carrying full-length *nes* in PstI and BamHI	This study
pSK6874	pSK5632 carrying *nes* loop 1 mutant (NRKNSQ→GS)	This study
pSK6875	pSK5632 carrying *nes* loop 2 mutant (KRKGNDYI→GS)	This study
pSK6876	pSK5632 carrying *nes* with premature stop codon (D304*)	This study

Bacterial cultures were grown with aeration at 37 °C in LB media unless stated otherwise. Antibiotics were used at the following concentrations: gentamicin (Gm), 20 μg/mL; neomycin (Nm), 15 μg/mL; tetracycline (Tc), 2 μg/mL; ampicillin (Ap), 100 μg/mL; erythromycin (Em), 10 μg/mL; and chloramphenicol (Cm), 10 μg/mL.

PCR and DNA sequencing. PCR was carried out under standard conditions, using Phusion High-Fidelity DNA polymerase (Finnzymes). Oligonucleotides were purchased from Geneworks Australia. DNA sequencing was performed by the Australian Genome Research Facility (Sydney).

Targeted disruption of pSK41 nes. An *nes* gene knockout was generated using the *Lactococcus lactis* Ll.LtrB group II intron of the Targetron system (14). Potential target sites in the *nes* coding region were identified using Intron Finder software (17). The chosen target site was at the 5′ end of *nes* between base pairs 41 and 42 of the coding region and in the antisense orientation. The pNL9164 intron (14) was used as a template in PCR to amplify two regions of the intron with primers Nes2-IBS (5′-AAA AAA GCT TAT AAT TAT CCT TAC TTT GCC CAT TTG TGC GCC CAG ATA GGG TG-3′) and EBS universal (5′-CGA AAT TAG AAA CTT GCG TTC AGT AAA C-3′) and Nes2-EBS2 (5′-TGA ACG CAA GTT TCT AAT TTC GGT TCA AAG TCG ATA GAG GAA AGT GTC T-3′) and Nes2-EBS1d (5′-CAG ATT GTA CAA ATG TGG TGA TAA CAG ATA AGT CCC ATT TGC TAA CTT ACC TTT CTT TGT-3′). The resulting PCR products were gel-purified with the Wizard SV gel and PCR clean-up system (Promega) and combined for overlap extension PCR, which included only primers Nes2-IBS and Nes2-EBS1d. The resulting ∼350-bp fragment was cloned into the BsrGI and HindIII sites of pNL9164, effectively engineering the intron (originally targeting *hsa*) to target *nes*. The modified region of the resulting plasmid pNL9164-nes2 was sequenced using the Targetron-Fwd primer (5′-CTT TAG GTG ATG AAC ATA TC-3′). pNL9164-nes2 was introduced into *S. aureus* RN4220 by electroporation, using a BioRad Genepulser set at 1.3 kV (25 μFD, 100 Ω), and transformants were selected on NYE agar (18) containing Em and incubated at 32 °C (pNL9164 carries a pT181 temperature-sensitive replicon). A single Em^R transformant was used as a recipient in matings (carried out at 32 °C) with SK5428 carrying pSK41. A resulting Nm^R, Gm^R, Em^R transconjugant was then cultured in LB until OD_{600} ∼ 0.5 and induced with cadmium chloride (10 μM) for 90 min. Serial dilutions of the culture were spread onto selective media and individual colonies were screened for *nes* insertions by colony PCR (lysis induced with lysostaphin), using the primers nes-1 (5′-GAT TTT ATT ATG GCA ATG TAC C-3′) and nes-2 (5′-GTC TAT CCT CTA TAT CCT C-3′). In the screen, the wild-type *nes* gene generated a 0.9-kb product and *nes* with an intron insertion generated a 1.8-kb product. One intron insertion was confirmed by sequencing the 1.8-kb PCR product. The strain carrying this insertion was cured of pNL9164-nes2 and designated SK6872 carrying pSK41::nes2.

Construction of nes complementation plasmids. The *nes* coding region, including the ribosome-binding site, was PCR amplified using the primers NesF-PstKpn (5′-CAG GTA CCT GCA GTC GCC TTC GCT CAA TAT TTG-3′) and NesR-Bam (5′-CAG GAT CCT GAA AAC AAA CAA GAA GAA GAA ATT G-3′). The resulting ∼2.0-kb product was digested with PstI and BamHI and cloned into the respective sites of pSK5632 in which *nes* transcription was driven by a *lac* promoter (16). A plasmid clone with the correct restriction profile was validated by sequencing the entire *nes* region. Equivalent *nes* constructs carrying the loop 1 deletion (NRKNSQ→GS), the loop 2 deletion (KRKGNDYI→GS), and a frameshift mutation in codon Q297 that introduces a premature stop codon (D304*; identical to that carried by plasmid pUSA03) were generated separately in pSK5632. For the loop 1 construct, *nes* was PCR amplified as two fragments using primers Nes-L1F (5′-GAT GTT GAG GGT TCA GTT GCA CGA GAA ATT ATA ATT GG-3′) and NesR-Bam and NesF-PstKpn and Nes-L1R (5′-CGT GCA ACT GAA CCC TCA ACA TCA TGA ACT TTA TTC C-3′). The products were gel-purified and combined as a template for overlap extension PCR, using primers NesR-Bam and NesF-PstKpn. The *nes* loop 2 and STOP mutations were created in a similar way, using Nes-L2F (5′-GAA TTT GAA CCT GGT TCA AGA GAT TGG AAT ACA AAA G-3′) and Nes-L2R (5′-CCA ATC TCT TGA ACC AGG TTC AAA TTC ATT ATT TTT ATC-3′) and Nes-STOPF (5′-GAC TAT ATG ATT TAA AAC AAA AAA ACT TCA TTA ATC AC-3′) and Nes-STOPR (5′-GTG ATT AAT GAA GTT TTT TTG TTT TAA ATC ATA TAG TC-3′), respectively. All three of the final PCR products were cloned into the PstI and BamHI sites of pSK5632 and sequenced. These plasmids were subsequently introduced into SK6872 by electroporation.

Conjugation experiments. Donor and recipient cultures were inoculated by placing a freshly grown single colony into 10 mL of LB and growing overnight with aeration. The cultures were then diluted 1:100 into 10 mL of fresh media and growth was continued to an OD_{600} of ∼0.6. Cells were pelleted and resuspended in 1 mL LB. Cells grown in the presence of antibiotics for plasmid selection (complementation experiments) were washed an additional two times with 1 mL LB. Matings were performed on a solid surface that was prepared by placing a sterile 2.5-cm^2 nylon membrane onto an LB plate. One-hundred–microliter aliquots of donor and recipient cell suspensions were mixed and placed onto the membrane. Once the liquid was absorbed, the plates were incubated upside down at 37 °C for 20 h. The membrane was placed into a sterile 10-mL tube and 1.0 mL of LB was added. Cells were suspended by vigorous vortexing and 100-μL aliquots were plated onto media selective for transconjugants. Serial dilutions of the cell suspensions were also plated onto media selective for the donor cells to calculate conjugation frequency.

Polyamide Synthesis. Polyamides were synthesized using microwave-assisted solid-phase synthesis on oxime resin as reported previously. Following cleavage from oxime resin, compounds were purified by preparative HPLC. The identity and purity of each polyamide were confirmed by MALDI-TOF and analytical HPLC analysis.

Match Polyamide **1** *ImβImPy-(R)*$^{\alpha\text{-}NH2}$*γ-PyβImPy-(+)*: MS (MALDI-TOF) calculated for $C_{50}H_{70}N_{21}O_{19}$ $[M+H]^+$ 1108.6, found 1108.9.

Mismatch Polyamide **2** *ImImImPy-(R)$^{\alpha\text{-}NH2}$γ-PyPyPyPy-(+)*: MS (MALDI-TOF) calculated for $C_{56}H_{72}N_{23}O_9$ $[M+H]^+$ 1210.6, found 1209.9.

DNA Duplex Melting Temperature Analysis. Melting temperature analysis was performed on a Varian Cary 100 spectrophotometer equipped with a thermo-controlled cell holder possessing a cell path length of 1 cm. An aqueous solution of 10 mM sodium cacodylate, 10 mM KCl, 10 mM $MgCl_2$, and 5 mM $CaCl_2$ at pH 7.0 was used as an analysis buffer. Oligonucleotides (0.1-mM stock solutions dissolved in 10 mM Tris·Cl, 0.1 mM EDTA, pH 8.0) were purchased from Integrated DNA Technologies. DNA duplexes and hairpin polyamides (**1** or **2**) were mixed to a final concentration of 1 μM and 1.2 μM, respectively, for each experiment. Before analysis, samples were heated to 90 °C and cooled to a starting temperature of 25 °C with a heating rate of 5 °C/min for each ramp. Denaturation profiles were recorded at λ = 260 nm from 25 °C to 90 °C with a heating rate of 0.5 °C/min. The reported melting temperatures were defined as the maximum of the first derivative of the denaturation profile and represent the average of two independent measurements. All melting temperature shifts (ΔT_m) are calculated relative to a standardized naked control oligonucleotide.

Polyamide Inhibition. Equilibrium DNA cleavage-religation assays were conducted in vitro with either the relaxase domains of NES (1–220) or the full-length enzyme as described above. For polyamide inhibition, 2.5 μL of 20 μM oriTHP37 DNA substrate was incubated with 2.5 μL of polyamide at 20× the reaction concentration or 100% DMSO for 15 min. Each reaction contained 1 μL of the incubated DNA mixture in place of the 1 μL of DNA alone previously used.

1. Otwinowski Z, Minor W (1997) Processing of X-ray diffraction data collected in oscillation mode. *Methods Enzymol* 276:307–326.
2. Adams PD, et al. (2010) PHENIX: A comprehensive Python-based system for macromolecular structure solution. *Acta Crystallogr D Biol Crystallogr* 66(Pt 2): 213–221.
3. Monzingo AF, Ozburn A, Xia S, Meyer RJ, Robertus JD (2007) The structure of the minimal relaxase domain of MobA at 2.1 A resolution. *J Mol Biol* 366(1):165–178.
4. Emsley P, Lohkamp B, Scott WG, Cowtan K (2010) Features and development of Coot. *Acta Crystallogr D Biol Crystallogr* 66(Pt 4):486–501.
5. Kabsch W (2010) XDS. *Acta Crystallogr D Biol Crystallogr* 66(Pt 2):125–132.
6. Nikolovska-Coleska Z, et al. (2004) Development and optimization of a binding assay for the XIAP BIR3 domain using fluorescence polarization. *Anal Biochem* 332(2):261–273.
7. Nikolovska-Coleska Z, et al. (2008) Design and characterization of bivalent Smac-based peptides as antagonists of XIAP and development and validation of a fluorescence polarization assay for XIAP containing both BIR2 and BIR3 domains. *Anal Biochem* 374(1):87–98.
8. Svergun DI (1999) Restoring low resolution structure of biological macromolecules from solution scattering using simulated annealing. *Biophys J* 76(6):2879–2886.
9. Pettersen EF, et al. (2004) UCSF Chimera—a visualization system for exploratory research and analysis. *J Comput Chem* 25(13):1605–1612.
10. Petoukhov MV, Svergun DI (2005) Global rigid body modeling of macromolecular complexes against small-angle scattering data. *Biophys J* 89(2):1237–1250.
11. Kreiswirth BN, et al. (1983) The toxic shock syndrome exotoxin structural gene is not detectably transmitted by a prophage. *Nature* 305(5936):709–712.
12. Lyon BR, May JW, Skurray RA (1984) Tn4001: A gentamicin and kanamycin resistance transposon in Staphylococcus aureus. *Mol Gen Genet* 193(3):554–556.
13. Liu MA, Kwong SM, Pon CK, Skurray RA, Firth N (2012) Genetic requirements for replication initiation of the staphylococcal multiresistance plasmid pSK41. *Microbiology* 158(Pt 6):1456–1467.
14. Yao J, et al. (2006) Use of targetrons to disrupt essential and nonessential genes in Staphylococcus aureus reveals temperature sensitivity of Ll.LtrB group II intron splicing. *RNA* 12(7):1271–1281.
15. Berg T, et al. (1998) Complete nucleotide sequence of pSK41: Evolution of staphylococcal conjugative multiresistance plasmids. *J Bacteriol* 180(17):4350–4359.
16. Grkovic S, Brown MH, Hardie KM, Firth N, Skurray RA (2003) Stable low-copy-number Staphylococcus aureus shuttle vectors. *Microbiology* 149(Pt 3):785–794.
17. Carter GP, et al. (2011) TcsL is an essential virulence factor in Clostridium sordellii ATCC 9714. *Infect Immun* 79(3):1025–1032.
18. Schenk S, Laddaga RA (1992) Improved method for electroporation of Staphylococcus aureus. *FEMS Microbiol Lett* 73(1–2):133–138.

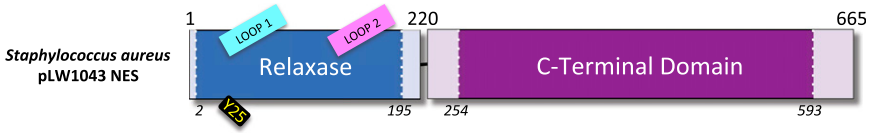

Fig. S1. Domain architecture of *S. aureus* pLW1043 NES. Relaxase and C-terminal regions of NES are shown, with the domains elucidated structurally highlighted by dashed lines. The locations of the relaxase catalytic tyrosine (Y25), as well as DNA-binding loops 1 and 2, are indicated.

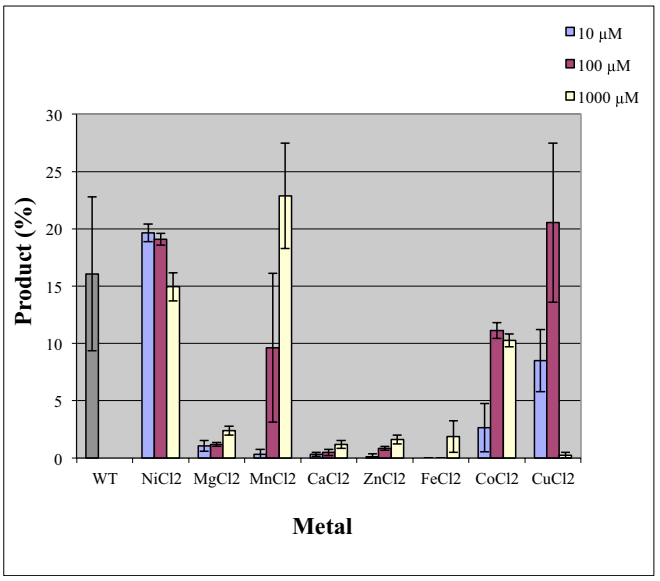

Fig. S2. Equilibrium DNA cleavage with divalent metals. Percentage of product formation is shown for wild-type NES relaxase 1–220 with the indicated concentrations of eight divalent metal compounds and using *oriTHP37* as a substrate (Table S4). The NES relaxase was treated with metal chelator before the addition of the exogenous metals indicated.

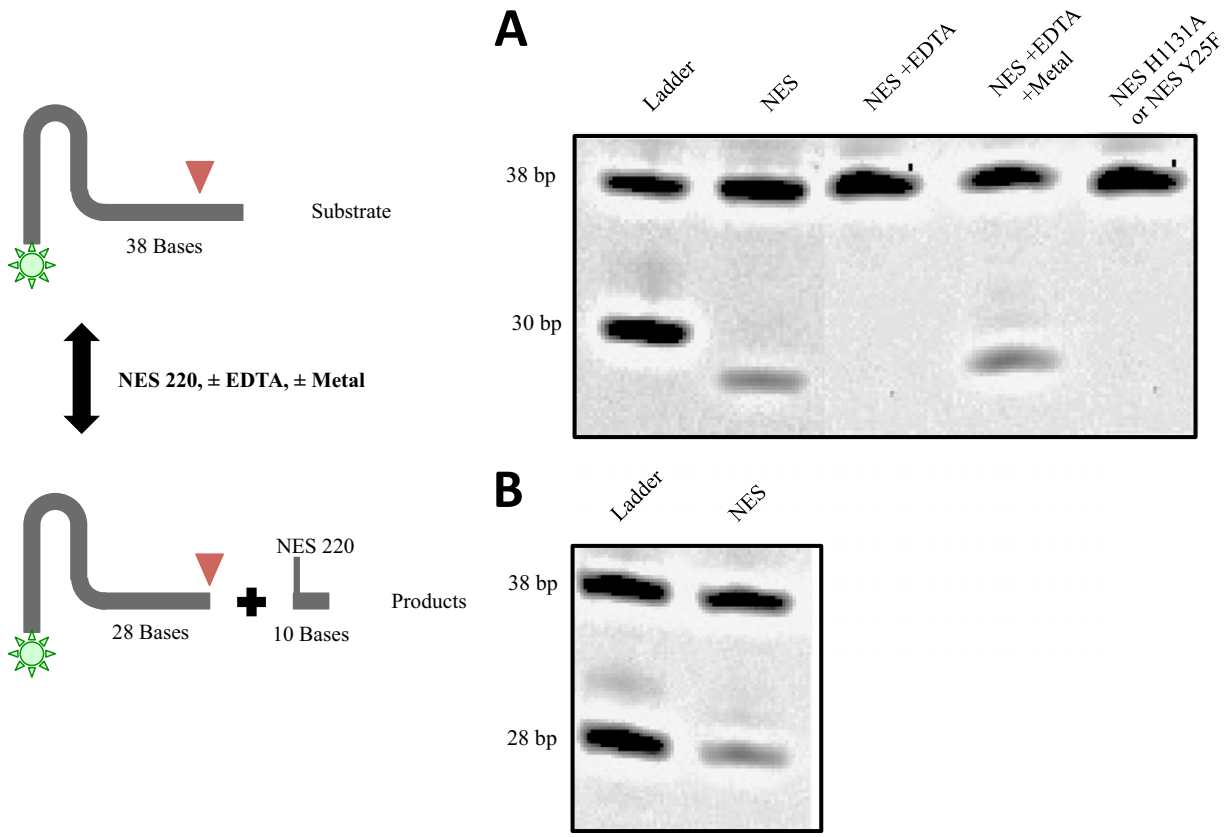

Fig. S3. DNA cleavage assay to determine the *nic* site. The schematic shows wild-type NES relaxase 1–220 (NES 220) was used and a substrate oligo 38 nt in length (one longer than *oriTHP37*, Table S4). The *nic* site is indicated by a red arrowhead and the 6FAM fluorophore by a green star. (*A*) On the basis of published work on the highly related pGO1 NES enzyme (1), a 30-nt product was expected (Ladder). Instead, NES produced a 28-nt fluorescently labeled product, but only when the catalytic Tyr-25 was intact (Y25) and when a divalent metal (Ni) was present. (*B*) The 28-nt product was confirmed using a ladder with 5′-labeled 6FAM 28- and 38-nt oligos.

1. Climo MW, Sharma VK, Archer GL (1996) Identification and characterization of the origin of conjugative transfer (oriT) and a gene (nes) encoding a single-stranded endonuclease on the staphylococcal plasmid pGO1. *J Bacteriol* 178(16):4975–4983.

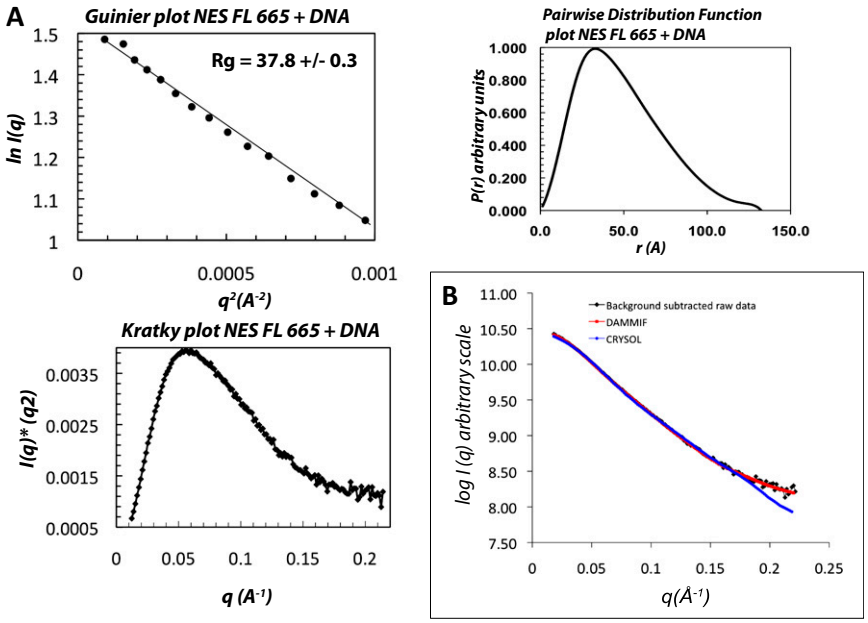

Fig. S4. Small-angle X-ray scattering analysis. Shown is the information suggested by Jacques et al. (1) for publishing small-angle scattering data from biomolecules. (*A*) The Guinier plot (*Upper Left*) was generated using PRIMUS (2) to calculate the radius of gyration (R_g) of 37.8 Å for full-length NES 1–665 bound to DNA oligo oriTHP30 (Table S4). The AutoGNOM (3) algorithm in PRIMUS was used to generate the pairwise distribution function (*Upper Right*, arbitrary units), using a D_{max} of 129 Å. The R_gs calculated by the Guinier and GNOM methods agree within 1 Å. The Kratky plot (*Lower Left*, also generated by PRIMUS) shows properties consistent with a folded protein. (*B*) The three curves show the background-subtracted raw scattering data on a log Intensity vs. *q*-scale (black diamonds) compared with both the calculated curves for the two-phase (protein and DNA) dummy atom model generated by MONSA (4) (calculated chi fit score = 1.16, red squares) and the SASREF (5) rigid-body fit model shown in Fig. 3*D* (calculated chi fit score = 3.82, blue). The deviation in fit at higher *q* in the rigid body model (blue curve vs. black) reflects the fact that we are missing 130 residues in the crystal structures that are present in the protein used for the SAXS scattering, as well as inaccuracies in the rigid-body fit model in terms of relative orientation of the two domains.

1. Jacques DA, Guss JM, Svergun DI, Trewhella J (2012) Publication guidelines for structural modelling of small-angle scattering data from biomolecules in solution. *Acta Crystallogr D Biol Crystallogr* 68(Pt 6):620–626.
2. Konarev PV, Sokolova AV, Koch MHJ, Svergun DI (2003) PRIMUS: A Windows PC-based system for small-angle scattering data analysis. *J Appl Cryst* 36:1277–1282.
3. Svergum DI (1992) Determination of the regularization parameter in indirect-transform methods using perceptual criteria. *J Appl Cryst* 25:495–503.
4. Svergun DI (1999) Restoring low resolution structure of biological macromolecules from solution scattering using simulated annealing. *Biophys J* 76(6):2879–2886.
5. Petoukhov MV, Svergun DI (2005) Global rigid body modeling of macromolecular complexes against small-angle scattering data. *Biophys J* 89(2):1237–1250.

	duplex	
	5'-TGGT **GCGAA** CCT-3'	
Polyamide	T_m / °C	ΔT_m / °C
—	59.2 (±1.3)	—
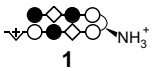 **1**	68.6 (±0.7)	9.3
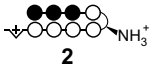 **2**	62.2 (±0.7)	2.9

Fig. S5. DNA thermal melting with polyamides. Shown is melting temperature (T_m) of the DNA duplex alone and with the Match and Mismatch Polyamides (**1** and **2**, respectively). The change in T_m is also indicated. One strand of the duplex oligo is shown, with the target sequence depicted in blue.

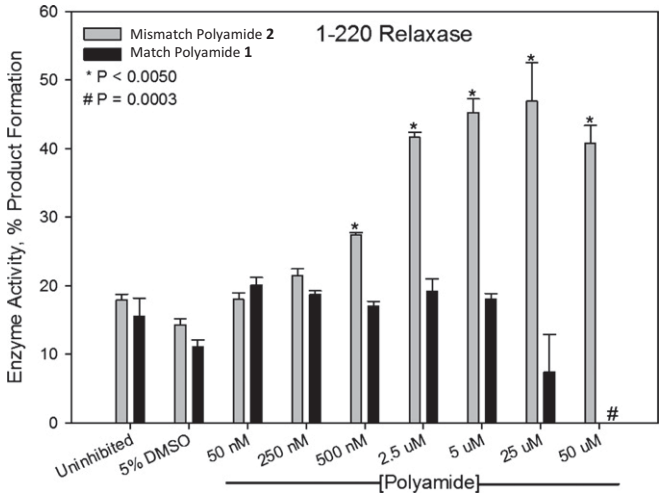

Fig. S6. Polyamide impact on NES relaxase activity. Shown is inhibition of NES relaxase in vitro with Match Polyamide **1** (black) and Mismatch Polyamide **2**. Polyamides were dissolved in 5% DMSO.

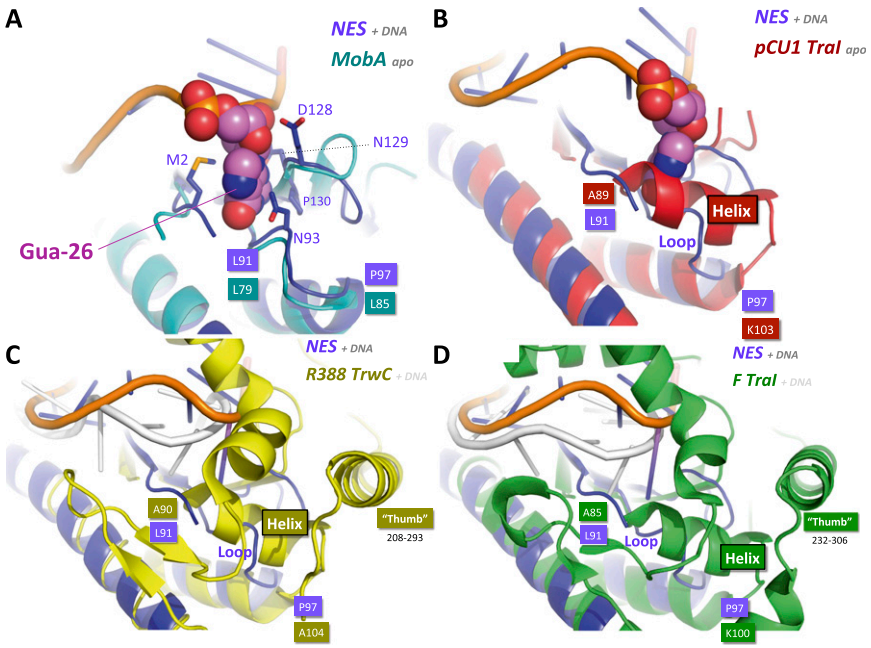

Fig. S7. Structural analysis of Gua-26 binding by NES. (*A*) Gua-26 is buried in the NES relaxase–DNA complex crystal structure between residues M2, N93, and amino acids 128–130 (D, N, and P, respectively). The region between L91 and P97 is a short loop in NES. Superposition of the structure of the MobA protein from plasmid R1162, which is a "single-tyrosine" relaxase like NES, in an apo (without DNA) state (cyan) on the structure of the NES–DNA complex (purple for protein regions) is also shown. The region between L79 and L85 is a short loop in MobA (1). (*B*) Superposition of the structure of the TraI protein from plasmid pCU1, which is a "multityrosine" relaxase, in an apo (without DNA) state (red) on the structure of the NES–DNA complex (purple for protein regions). The region between A89 and K103 is a helix in pCU1 TraI (2) that occludes the Gua-26 binding site in NES. The superimposed molecules have been rotated ~30° about the vertical axis in *B*, *C*, and *D* relative to *A*. (*C*) Superposition of the structure of the TrwC protein from plasmid R388 (yellow), which is a multityrosine relaxase, complexed with DNA (white) on the structure of the NES–DNA complex (purple for protein regions, orange for DNA backbone). The region between A90 and A104 is a helix in TrwC (3) that occludes the Gua-26 binding site in NES. The "Thumb" region (residues 208–293) unique to TrwC (yellow) relative to NES (purple) is indicated. (*D*) Superposition of the structure of the TraI protein from the F plasmid (green), which is a multityrosine relaxase, complexed with DNA (white) on the structure of the NES–DNA complex (purple for protein regions, orange for DNA backbone). The region between A85 and K100 is a helix in F plasmid TraI (4) that occludes the Gua-26 binding site in NES. The Thumb region (residues 232–306) unique to F TraI (green) relative to NES (purple) is indicated.

1. Monzingo AF, Ozburn A, Xia S, Meyer RJ, Robertus JD (2007) The structure of the minimal relaxase domain of MobA at 2.1 A resolution. *J Mol Biol* 366(1):165–178.
2. Nash RP, Habibi S, Cheng Y, Lujan SA, Redinbo MR (2010) The mechanism and control of DNA transfer by the conjugative relaxase of resistance plasmid pCU1. *Nucleic Acids Res* 38(17): 5929–5943.
3. Guasch A, et al. (2003) Recognition and processing of the origin of transfer DNA by conjugative relaxase TrwC. *Nat Struct Biol* 10(12):1002–1010.
4. Larkin C, et al. (2005) Inter- and intramolecular determinants of the specificity of single-stranded DNA binding and cleavage by the F factor relaxase. *Structure* 13(10):1533–1544.

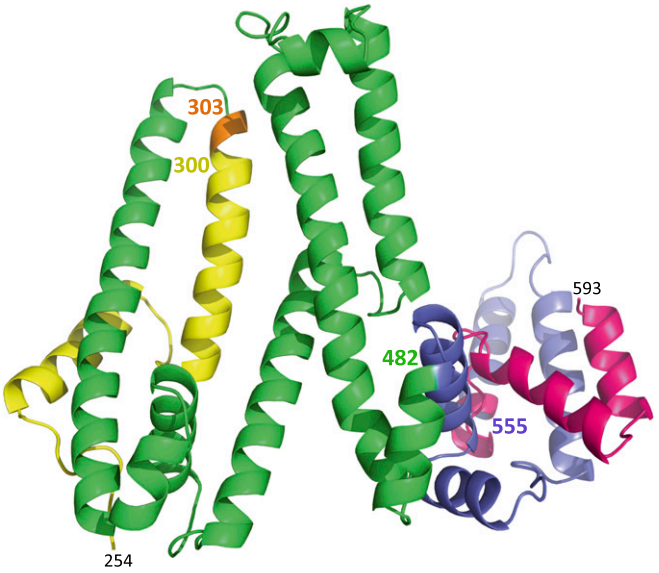

Fig. S8. Truncated forms of NES C-terminal domain sequenced. The C-terminal domain of pLW1043 NES (residues 254–593) is shown as in Fig. 1*C* with the sites of truncation indicated for four forms of *Staphylococcus aureus* NES sequenced. Proteins terminating at residues 300 (yellow, accession no. CCJ09841), 303 (orange, YP_492718), 482 (green, ADM29113) (1), and 555 (purple, EIK19451) are highlighted, with the remaining structured region of the C-terminal domain presented here rendered in magenta. Note that the NES from plasmid pUSA03 truncated by a premature stop codon at residue 303 (2) was used in the conjugation assays presented in Fig. 4*A*.

1. Diep BA, et al. (2006) Complete genome sequence of USA300, an epidemic clone of community-acquired meticillin-resistant Staphylococcus aureus. *Lancet* 367(9512):731–739.
2. Kennedy AD, et al. (2010) Complete nucleotide sequence analysis of plasmids in strains of Staphylococcus aureus clone USA300 reveals a high level of identity among isolates with closely related core genome sequences. *J Clin Microbiol* 48(12):4504–4511.

Table S1. Crystallographic statistics

	Relaxase–DNA complex		C-terminal domain	
Data collection				
Space group	$P6_422$		$P4_32_12$	
Cell dimensions				
a, *b*, *c*, Å	63.2, 63.2, 314		75.7, 75.7, 181	
α, β, γ, °	90, 90, 120		90, 90, 90	
	Inflection	Peak	Inflection	Remote
Wavelength	0.95471	0.97926	0.97949	0.94928
Resolution, Å	48.5–2.90 (2.90–2.95)*	100–3.0 (3.05–3.00)*	100–3.0 (3.05–3.00)*	100–3.0 (3.05–3.00)*
R_{merge}	0.097 (0.26)	0.095 (0.52)	0.085 (0.48)	0.09 (0.51)
$I/\sigma I$	48 (5.9)	26 (2.0)	29.4 (2.8)	29 (2.5)
Completeness, %	97.7 (79.7)	99.7 (100.0)	99.7 (100)	99.7 (100)
Redundancy	20.3 (13.2)	9.4 (9.7)	9.4 (9.7)	9.4 (9.7)
Refinement				
Resolution, Å	49–2.9		45.8–3.0	
No. reflections	8,824		10,958	
R_{work}/R_{free}	0.229/0.286		0.261/0.284	
No. atoms				
Total	2,166		5,081	
Ligand/ion	13 (9 Ca, 1 Cl, 1 Ni, 2 Se)		1 Ca, 5 Se	
Water	19		0	
Isotropic *B*-factors, ave., $Å^2$				
Protein	76		70.5	
Ligand/ion/DNA	76.8		62.3	
Water	67.4		NA	
rms deviations				
Bond lengths, Å	0.003		0.003	
Bond angles, °	0.74		0.84	

One crystal was used for each structure. NA, not applicable.
*Values in parentheses are for highest-resolution shell.

Table S2. ICP-MS analysis of metal binding to NES 1–220

	NES 1–220 Y25F, %	NES 1–220 Y25F, H131A, %
Ni	20.28	0.16
Mg	0.75	1.40
Mn	0.00	0.01
Ca	0.24	0.44
Zn	2.85	0.11
Fe	0.32	0.39

The presence of six divalent metal ions associated with two forms of the relaxase domain (residues 1–220) of NES, a catalytic Try25Phe mutant (NES 220 Y25F) and a double mutant in which one of the metal-chelating histidines, His131, was replaced with alanine (NES 220 Y25FH131A), was examined by inductively coupled plasma mass spectrometry (ICP-MS).

Table S3. DNA binding by NES relaxase

	5′ oligonucleotides 3′	Values
	Direct DNA binding	K_D, nM
6FAM-oriT31	6FAM-CACGCGAACGGAACGTTCGCATAAGTGC**GC***C*	18.2 ± 2.7
	Competition shifted 30 nt DNA binding	K_i, nM
oriTHP30(-2)	GCACGCGAACGGAACGTTCGCATAAGTGC**G**	307 ± 46
oriTHP30(-1)	CACGCGAACGGAACGTTCGCATAAGTGC**GC**	14.5 ± 2.2
oriTHP30	ACGCGAACGGAACGTTCGCATAAGTGC**GC***C*	7.9 ± 1
oriTHP30(+1)	CGCGAACGGAACGTTCGCATAAGTGC**GC***CC*	9.0 ± 1
oriTHP30(+2)	GCGAACGGAACGTTCGCATAAGTGC**GC***CCT*	4.0 ± 0.6
oriTHP30(+3)	CGAACGGAACGTTCGCATAAGTGC**GC***CCTT*	13.9 ± 2.1
oriTHP30(+4)	GAACGGAACGTTCGCATAAGTG**CGC***CCTTA*	16.5 ± 2.5
oriTHP30(+5)	AACGGAACGTTCGCATAAGTGC**GC**CCTTAC	NC
	Competition truncated DNA binding	K_i, nM
(-2)oriT27	GAACGGAACGTTCGCATAAGTGC**GC***CC*	1,060 ± 160
(-5)oriT24	CGGAACGTTCGCATAAGTGC**GC**CC	NC
(-7)oriT22	GAACGTTCGCATAAGTGC**GC**CC	NC
oriT27	CGCGAACGGAACGTTCGCATAAGTGC**G**	5.8 ± 0.02
oriT24(-3)	CGCGAACGGAACGTTCGCATAAGT	97.5 ± 0.029
oriT21(-6)	CGCGAACGGAACGTTCGCATA	821 ± 122
oriT18(-9)	CGCGAACGGAACGTTCGC	NC
	Competition mutation DNA binding	K_i, nM
oriTnoHP29	AC**CTATCGT**GAACGTTCGCATAAGTGC**GC**	553 ± 82
oriTHP30T21A	ACGCGAACGGAACGTTCGCA**A**AAGTGC**GC**CC	84.8 ± 13
T21C	ACGCGAACGGAACGTTCGCA**C**AAGTGC**GC**CC	135 ± 20
T21G	ACGCGAACGGAACGTTCGCA**G**AAGTGC**GC**CC	521 ± 77
oriTHP30A20T	ACGCGAACGGAACGTTCGC**T**TAAGTGC**GC**C	78.7 ± 12
A20C	ACGCGAACGGAACGTTCGC**C**TAAGTGC**GC**C	95.9 ± 14
A20G	ACGCGAACGGAACGTTCGC**G**TAAGTGC**GC**C	440 ± 54
oriTHP304:18CG-GC	AC**GG**GAACGGAACGTTC**C**CATAAGTGC**GC**C	NC
CG-AT	AC**A**GAACGGAACGTTC**T**CATAAGTGC**GC**C	NC
CG-TA	AC**T**GAACGGAACGTTC**A**CATAAGTGC**GC**C	213 ± 32
oriTHP305:17GC-CG	AC**C**CAACGGAACGTT**G**GCATAAGTGC**GC**C	292 ± 43
GC-AT	AC**A**AACGGAACGTTT**G**CATAAGTGC**GC**C	23.9 ± 3.6
GC-TA	AC**T**AACGGAACGTT**A**GCATAAGTGC**GC**C	89.6 ± 13
oriTHP33Loop(+3)	ACGCGAACG**C**GAA**TC**CGTTCGCATAAGTGC**GC**C	51.0 ± 7.6

Shown are DNA oligonucleotides examined by fluorescence polarization anisotropy for binding to the relaxase 1–220 form of NES. Both direct binding, using a 6FAM–5′-labeled oligo (*6FAMoriT31*, where *oriT* denotes the origin of transfer element), and indirect competition binding were examined. Oligos are named according to their length, shift in sequence relative to *oriT31,* and presence of hairpin (HP). Numbering is according to Fig. 2*A*. The *oriTHP30* oligo was used in the crystal structure of the NES relaxase–DNA complex presented here. An underline corresponds to the bases involved in formation of the DNA hairpin. Bases in boldface type correspond to the true *nic* site whereas italicized bases represent the hypothesized *nic* site. Bases in boldface type are mutations made to the WT sequence for oligos 17–30. NC, not a competitor.

Table S4. Oligos used in NES activity assays

	Relaxase activity substrate oligos
*oriTHP**37***	6FAM-ACGCGAACGGAACGTTCGCATAAGTGC**GC**CCTTACGG
*oriTHP**36***	6FAM-ACGCGAACGGAACGTTCGCATAAGTGC**GC**CCTTACG
*oriTHP**35***	6FAM-ACGCGAACGGAACGTTCGCATAAGTGC**GC**CCTTAC
*oriTHP**34***	6FAM-ACGCGAACGGAACGTTCGCATAAGTGC**GC**CCTTA
*oriTHP**33***	6FAM-ACGCGAACGGAACGTTCGCATAAGTGC**GC**CCTT
*oriTHP**32***	6FAM-ACGCGAACGGAACGTTCGCATAAGTGC**GC**CCT
*oriTHP**31***	6FAM-ACGCGAACGGAACGTTCGCATAAGTGC**GC**CC
*oriTHP**30***	6FAM-ACGCGAACGGAACGTTCGCATAAGTGC**GC**C
*oriT**noHP**37*	6FAM-AC***CTATCGT***GAACGTTCGCATAAGTGC**GC**CCTTACGG
*oriTHP37**T21G***	6FAM-ACGCGAACGGAACGTTCGCA***G***AAGTGC**GC**CCTTACGG
*oriTHP37**A20G***	6FAM-ACGCGAACGGAACGTTCGC***G***TAAGTGC**GC**CCTTACGG
*oriTHP37**4:18CG-GC***	6FAM-ACG***G***GAACGGAACGTTC**C**CATAAGTGC**GC**CCTTACGG
*oriTHP37**5:17GC-AT***	6FAM-ACGC***A***AACGGAACGTT***T***GCATAAGTGC**GC**CCTTACGG
*oriTHP37**abasicG26***	6FAM-ACGCGAACGGAACGTTCGCATAAGT_C**GC**CCTTACGG
*oriTHP**40***	6FAM-ACGCGAACGGAACGTTCGCATAAGTGC**GC**CCTTACGGGAT
*oriTHP**45***	6FAM-ACGCGAACGGAACGTTCGCATAAGTGC**GC**CCTTACGGGATTTAAC

The GC bases in boldface type are the relaxase's *nic* site. Underlines correspond to the DNA hairpin. 6-FAM shows the location of the fluorescein label. Bases in boldface type other than the *nic* site represent changes made relative to the normal plasmid sequence. *OriT* denotes the origin of transfer element, and HP the DNA hairpin motif. Nucleotides are numbered according to Fig. 2*A*, and shown 5′ to 3′.

Table S5. DNA binding by NES using 6FAM-*oriTHP30*

	$K_d \pm$ SD, nM
NES 1–220 Y25F	18.2 ± 2.7
Y25F + K22A	9.00 ± 1.6
Y25F + E86A	NS
Y25F + A21E	13.4 ± 3.2
Y25F + Loop1Δ	NS
Y25F + Loop2 Δ	118 ± 44*
NES 1–665 Y25F	1.37 ± 0.56

Shown is direct DNA binding measured by fluorescence polarization anisotropy for the indicated forms of NES to a *6FAM-oriTHP30* oligo (Table S3). NS, nonspecific DNA binding.
*R^2 = 0.86 for the Y25F with the deletion (Δ) of relaxase loop 2, indicating a poor fit due to nearly nonspecific binding.